Physics of Fluids

RESEARCH ARTICLE | APRIL 12 2023

Experimental study of a dental airotor cooling spray system

Binita Pathak ; Saurabh Yadav

Physics of Fluids 35, 042107 (2023)
https://doi.org/10.1063/5.0143781

Physics of Fluids ARTICLE scitation.org/journal/phf

Experimental study of a dental airotor cooling spray system

Cite as: Phys. Fluids **35**, 042107 (2023); doi: 10.1063/5.0143781
Submitted: 26 January 2023 · Accepted: 28 March 2023 ·
Published Online: 12 April 2023

Binita Pathak[a] and Saurabh Yadav

AFFILIATIONS

Department of Mechanical Engineering, Indian Institute of Technology, IIT-BHU Varanasi, Varanasi 221005, India

[a]**Author to whom correspondence should be addressed:** binita.mec@itbhu.ac.in and binitapathak88@gmail.com.
Tel.: +91-8105431120

ABSTRACT

In this paper, we have characterized a spray system used in dental airotors. Experimental data with respect to droplet size and velocity are generated at different locations in the spray. The impact dynamics of the spray upon substrates are also analyzed. The breakup modes have been identified in the system, and appropriate physical insights into the dynamics are provided. The impact of the spray upon both the hard substrates results in highly rebounding daughter droplets, which can contribute to bio-aerosols. The risks of cross-contamination due to aerosol can thus be prevented with appropriate modifications of the spray nozzles.

I. INTRODUCTION

Aerosols created during regular activities like speaking, coughing, sneezing, etc., can lead to the transmission of highly contagious disease.[1] The possibility of transmission of disease is very high in dental healthcare settings.[2–5] One such possibility of disease transmission is through the use of dental airotors. The airotors are rotary instruments which are routinely used for dental procedures like root canal treatment, plaques removal, fillings, prostheses, etc. The technology has evolved greatly in the last several decades in terms of rotor speed, cooling effect, maintenance, and visibility.[6] However, it is only recently that the scientific and the medical communities have realized the risks associated with aerosols created by airotors.[7–9] The airotors are operated at very high speed and require continuous cooling to prevent damage due to excessive heat produced in the treatment procedures. Usually, water sprays are employed for the cooling purpose. The sprayed droplets impinge on the tool as well as the teeth and mixes with salivary fluids.[10] These droplets are then ejected back from patient's oral cavity and contribute to microbial aerosols in dental healthcare environment.[3,8,9,11] Therefore, it is crucial to prevent or control the rebounce of the sprayed droplets to minimize infections in dental procedures. Modification of the coolant spray characteristics is one of the best possible methods to control the cross-contamination in dental environment. However, the spray characteristics associated with high-speed rotary instruments used in dental procedures have not been studied in detail so far.

A spray system is an integral part of many industries, such as ink-jet printing, coatings, combustion, agriculture, etc.[12] Different types of spray systems have been studied and developed over the years for different industrial applications.[13] For instance, uniform atomization of a spray is essential for obtaining desirable mixing and dispersion in many industrial processes. Therefore, several ways were identified to improve the atomization such as modification of the liquid properties (surface tension, viscosity, etc.).[14–16] Altering the liquid properties like surface tension also assists in NO_x reduction in fuel sprays employed in combustors.[16] The effect of variation of rheological properties is prominent upon the atomization of gel propellants.[17] A spray is a complex interplay of several instabilities such as Kelvin–Helmholtz, Rayleigh–Taylor, Rayleigh–Plateau, etc., which can lead to different modes of atomization and breakup such as bag breakup, surface stripping, secondary atomization, etc.[18–20] These complex interfacial interactions lead to a wide distribution in droplet sizes and velocities.[21] Therefore, understanding of the interfacial phenomena is crucial to obtain the desirable spatially and temporally distributed sprays. Accordingly, the modes of instabilities and breakups have been well explored in the context of industrial sprays. However, not much effort has been made toward the development of an efficient spray system in the field of medicine. The requirement of a spray system in medical field is different from the industrial spray systems. However, the understanding of an industrial atomizer can be utilized, and the designs can be engineered to be applicable in dentistry.

In this paper, we explore the characteristics of a spray system utilized to cool a dental airotor. The droplet size and velocity distributions are evaluated at different locations. We utilized high-speed photography to identify the breakup mechanisms in such sprays.

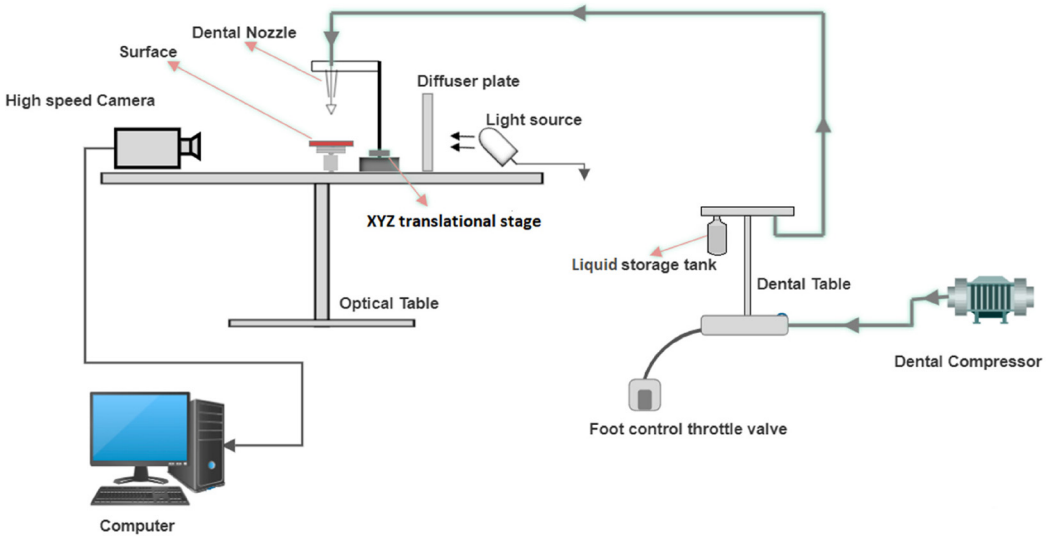

FIG. 1. Schematic of the experimental setup.

The droplets rebounding after impact mainly contributes to bio-aerosols. Therefore, understanding the impact dynamics is also equally important to prevent contamination. Sprays impacting a surface can result in several possible outcomes, such as adhesion, rebound, shattering, etc.[22] We report the dynamics of spray impact on substrates placed at different locations from the spray nozzle. The understanding of this work can be utilized to design a suitable spray system for dental airotors with the aim to reduce or eliminate cross-contamination in dental healthcare settings.

II. EXPERIMENTAL SETUP

The experimental setup is schematically shown in Fig. 1. The setup consists of a spray generated using a high-speed hand-held dental airotor. The airotor has one-hole water spray irrigation (Dentmark push button airotor handpiece-Shoo–121, operating within a speed range of 300 000–400 000 rpm). The compressed air used in the airotor was generated using oil-free dental compressor (model SE 750–40L-D, operating pressure 0–8 bar, storage tank capacity of 40 L, exhaust volume 135 LPM). The operation of the airotor was controlled through switch pedal. The spray was imaged using shadowgraphy technique. The spray dynamics were recorded at 30 000 fps (resolution: 1024 × 1024) using a high-speed camera (Photron Fastcam Mini AX100) attached with a zoom lens arrangement [8× Navitar lens combination with 2× Adapter tube (1–6030) and plan Apo 4× objective lens]. The spray was illuminated using a DC light source (Veritas Constellation 120e, with color temperature of 6200 K and a 15° beam angle lens.) along with the diffusor. The airotor was mounted on a XYZ translational stage in order to precisely control the movement. The set of experiments were performed to characterize the spray generated using the above-mentioned system. The minimum size of droplet that could be measured accurately using the current setup is about 10 μm.

The second set of experiments was performed to study the impact of the generated spray on surfaces. Glass slides of thickness of about ∼1.1 mm were used as the hard substrates. The region of impact on the glass slide was (13 mm × 7.5 mm). The substrate was placed on a Z-translation stage. The movement of both the surface and the airotor was precisely controlled to accurately position the region of interest in the focal plane of the camera. The entire setup was mounted on an optical table to avoid external vibrations and disturbances.

All the experiments were performed using de-ionized water spray as the working fluid. The experiments were carried out at the room temperature (30 °C) and a relative humidity of about 60%.

III. DESCRIPTION OF A DENTAL AIROTOR

The schematic of the dental airotor used in the experiments is shown in Fig. 2. The hand-piece consists of an air-driven turbine, which drives the tool (burr) used for dental treatments, such as removal of decay, fillings, prostheses, etc.[6] The exhaust air of the turbine exits through an orifice ["P_1" in Fig. 2(a)] at an angle of ∼28.2° (approximately). The pressurized water jet (maintained under 2 bar) exits the orifice (0.54 mm diameter) at an angle of about 45.5° from the surface ["P_2" in Fig. 2(a)]. Both the jets were operated using a throttle valve, and the experiments were performed under fully throttled condition.

The air jet interacts with the water jet outside the system and leads to the generation of the spray [Fig. 2(b)].This spray is used to cool the tool (burr) during dental operations. Throughout our experiments, the orientation of the airotor was kept such that the direction of the water jet coming out of airotor was vertically downward. The spray cone generated is, thus, skewed slightly at the tip of the cone by about 10° from the vertical axis (Table I).

IV. RESULTS AND DISCUSSION

The dynamics were identified using the high-speed recordings. The droplet images were tracked using a MATLAB code and ImageJ software. Only the droplets in focus were considered in all the analysis, and those which were not in the focal plane were not considered in the calculations. All the experiments were performed for 4 different trials in each case for repeatability.

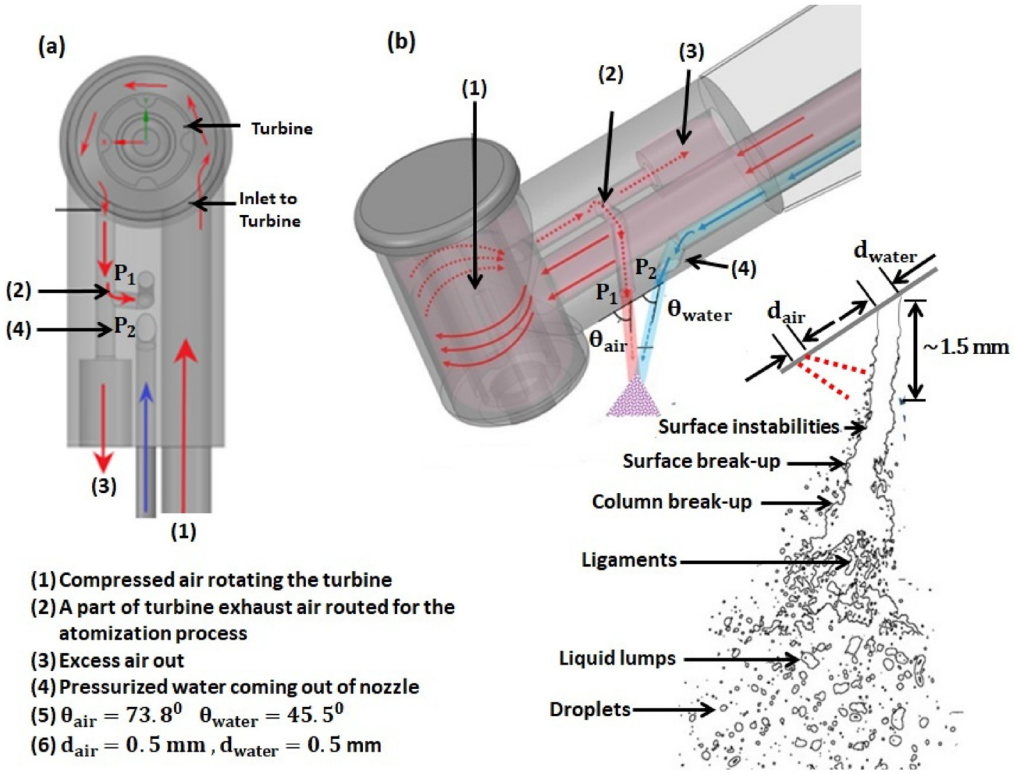

FIG. 2. Schematic of the dental airotor used in the current study: (a) top view and (b) side view.

A. Spray characterization

The spray system studied in this paper is a jet in crossflow type of system, which is typically employed in propulsion systems, agricultural sprays, etc.[2,3] The jet shows the characteristics of a typical liquid jet of low viscosity (Oh ∼ 0.005), which undergoes different types of breakup modes when subjected to a crossflow. The water jet coming out of the orifice ["o" in Fig. 3(a)] of the spray nozzle is cylindrical in shape and has a diameter of about (0.5 ± 0.02) mm. The jet flow rate is 0.001 kg/s. The pressurized air (∼200 kPa) is injected at a rate of 8.9×10^{-6} m^3/s, which interacts with the water jet at a distance of about (1.5 ± 0.1) mm from the center of the orifice [at o_1 in Fig. 3(a)]. In the first stage, the liquid column deflects in the streamwise direction of the crossflow followed by wavelike deformation of the column. The

TABLE I. The parameters of the spray system.

Nozzle diameter	0.5 mm
Air-hole diameter	0.5 mm
Liquid viscosity (μL)	0.001 kg/m s
Liquid density (ρL)	1000 kg/m^3
Liquid surface tension (σ)	0.07 N/m
Jet diameter (d0)	0.44 mm
Liquid Reynolds number $\left(\mathrm{Re_L} = \frac{\rho_L U_{jet} d_0}{\mu_L}\right)$	2300
Gas Weber number $\left(\mathrm{We_a} = \frac{\rho_a U_a^2 d_0}{\sigma}\right)$	13.7
Jet-crossflow momentum ratio $\left(\mathrm{M} = \frac{\rho_L U_{jet}^2}{\rho_a U_a^2}\right)$	6

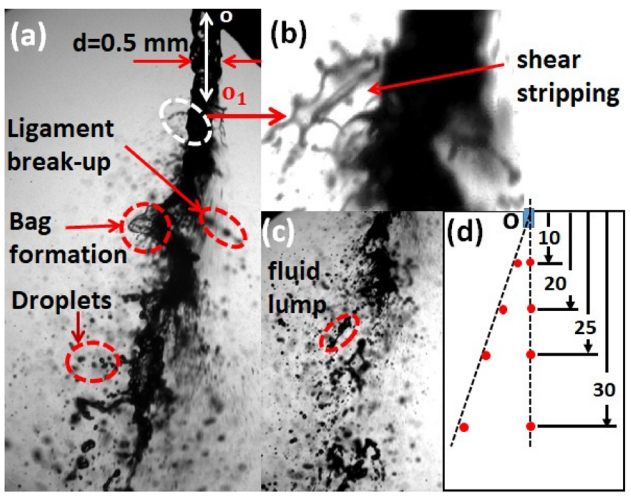

FIG. 3. (a) The jet breakup with the identified follow-up dynamics, (b) enlarged view of the peripheral region (the side view of the spray as the airotor is rotated by $\theta_{water} = 45.5°$ so that the water jet is along the vertical axis), (c) the spray structure after atomization, and (d) schematic of the locations of measurement in the spray (numbers represent the distance in mm from the nozzle exit).

jet deforms by $d_f/d_0 \sim 1.9$ (d_0: jet diameter and d_f: local width of jet at the point of breakup). The interaction of the air jet initiates instabilities in the water jet. This is evident by the shear-stripping of the jet into ligament-type structures (average length and width of the ligaments are $l_{lig} \sim 0.3$ mm, $d_{lig} \sim 0.03$ mm) at the periphery [Fig. 3(b)]. These ligaments grow due to its inertia and undergo Rayleigh–Plateau type breakup into droplets $\left(\frac{l_{lig}}{d_{lig}} \sim 9\right)$. The other breakup mode like bag formation was also identified (at a few locations) in the peripheral region [Fig. 3(a)], which expands and ruptures at its rim. The bag-breakup in a typical jet in crossflow occurs at low crossflow velocities (We $\sim$ 5). The rupture of bag leads to the formation of daughter droplets of various sizes. Some bag breakup also forms ligaments which undergo further breakup into droplets. The complete atomization of the jet into spray is achieved at a distance of about 15 mm below the orifice (o). The cone angle of the spray at that point is about 57° (±3°). Figure 3(c) depicts the spray structure which consists of droplets of multiple sizes as well as lumps of fluid (probably due to incomplete atomization of the ligaments) which moves with different velocities. The tiny droplets (mist-type) are observed mostly in the peripheral region due to complete atomization caused by shear stripping of the jet surface. The locations of measurements performed in this work are represented schematically in Fig. 3(d). The experiments were performed at four different locations (10–30 mm) from the nozzle exit (o) in the central plane as well as in the peripheral region of the spray.

B. Droplet size and velocity distribution

The distributions of droplets in the spray at different locations are shown in Fig. 4. The complete breakup of the jet occurs only beyond ~15 mm from the nozzle exit. Therefore, the spray near the nozzle exit (<15 mm) comprises mostly of incompletely atomized droplets. The deformed daughter droplets and liquid lumps formed due to recent breakup of the jet can be easily identified in the central region of the jet at a distance of 10 mm from the nozzle exit [Fig. 4(a)]. The aspect ratios of these droplets (AR) are typically about 1.5–5 [Fig. 5(a)]. These droplets are of various sizes with average diameters within a range of (50–350) μm [Fig. 5(b)]. The atomization is better as the spray progresses forward and the droplets undergo further breakup into smaller droplets at a distance greater than 15 mm from the nozzle exit [Fig. 4(b)]. The aspect ratios of these droplets are mostly within a range of 1.1–2 and are of an average diameter of 50–200 μm [Figs. 5(a) and 5(b)]. The spray is more uniform as it moves further away from the nozzle exit. It comprises of droplets which are mostly spherical (diameter, d $\sim$ 50–150 μm) [Figs. 4(c) and 5].

Alternatively, the jet surface (peripheral region) endures severe shear stripping due to interaction with the external air flow [Fig. 3(b)]. Therefore, the interface undergoes complete breakup into smaller droplets [diameter ~50 (±20) μm] which are mostly spherical in shape (AR $\sim$ 1), irrespective of the distance from the nozzle exit [Figs. 4(d)–4(f) and 5]. These droplets also traverse with a lower net velocity (~8 m/s) in the peripheral region due to high shear stress as compared

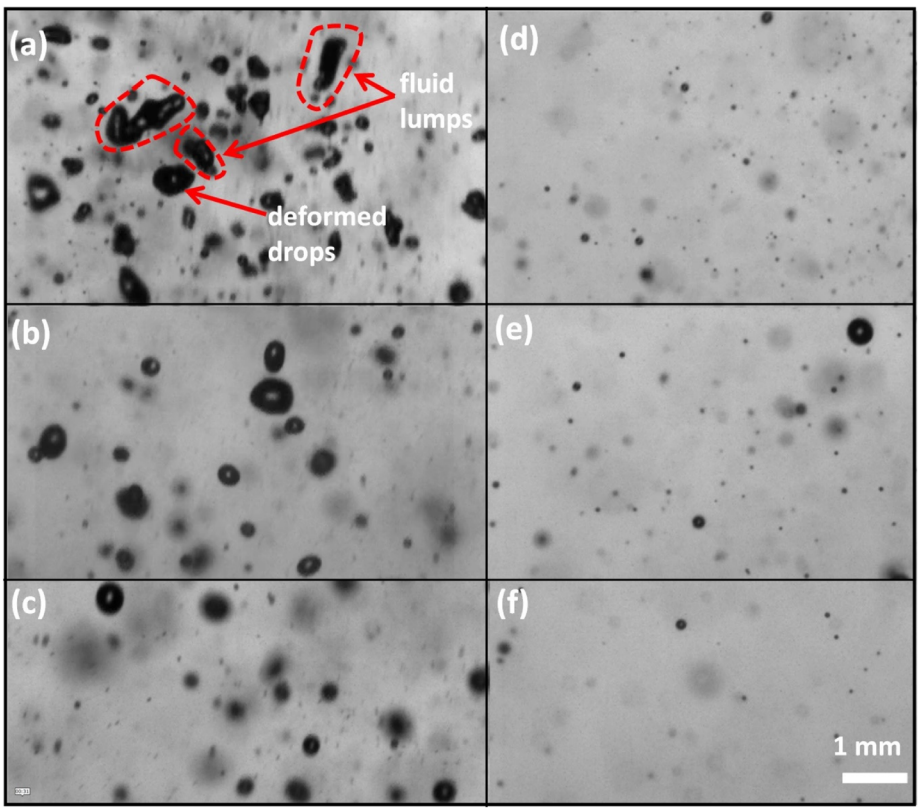

FIG. 4. Distribution of droplets in the central region of the spray at a distance of (a) 10, (b) 20, and (c) 30 mm from the nozzle exit. The right panel shows the distribution in the peripheral region at a distance of (d) 10, (e) 20, and (f) 30 mm from the nozzle exit.

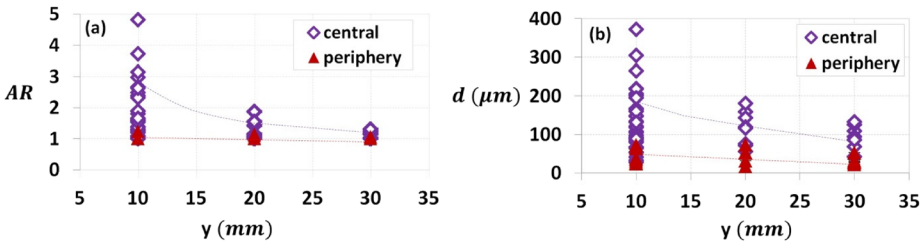

FIG. 5. Variation of (a) aspect ratio and (b) diameter of droplets in the spray with distance from the nozzle exit.

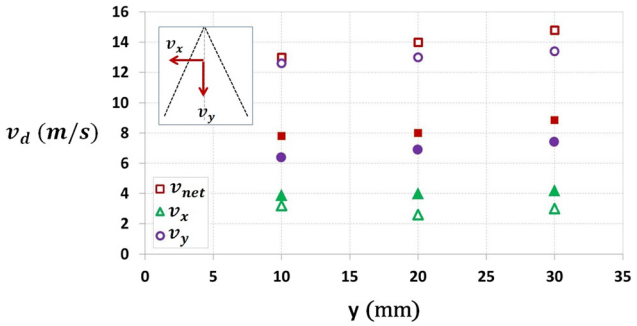

FIG. 6. Variation of the net velocity of the droplets (averaged over the range of droplet sizes in the spray) with distance from the nozzle exit (filled symbols represent droplets in the peripheral region of the spray and unfilled symbols represent droplets in the central region, respectively).

to that in the central region ($v_{net,central} \sim 2v_{net,peripheral}$) (Fig. 6). It is to be noted that the velocity is averaged over a range of droplet sizes in the spray. The energy of the droplets in this region thus reduces by about an order ($E_k \sim O(10^{-7})$ J) as compared to the droplets in the centerline region ($E_k \sim O(10^{-6})$ J). The orthogonal injection of the spray induces velocity in the stream-wise direction (v_y) to the droplets. However, the influence of air hitting the water jet also induces some drift velocity in the crosswise direction (v_x) to the droplets, although it is significantly smaller than v_y ($v_y \sim 4v_x$). The effect is more prominent at the periphery ($v_y \sim 1.7v_x$). As the droplets undergo continuous atomization, the average size reduces ($\frac{dd}{dy} \sim -2\,\mu m/mm$) as the spray moves further away from the nozzle exit [Fig. 5(b)]. The kinetic energy of the daughter droplets formed in the breakup process is given as $E_{kf} = E_{ki} - \sigma\pi d^2$ (here, E_{ki} is the kinetic energy of the droplet breaking up into droplets of diameter "d" and kinetic energy E_{kf}, σ is the surface tension). The surface energy ($\sigma\pi d^2$) required to form a new droplet is less than the kinetic energy by an order, which indicates that the droplets have kinetic energies of similar orders ($E_{kf} \sim E_{ki}$). Therefore, as the droplet size decreases with the distance, the velocity of these droplets increases. Accordingly, the velocity in the stream-wise direction (v_y) increases by $\sim 0.04\ ms^{-1}/mm$ as it moves away from the nozzle. Since the velocity in the crosswise direction (v_x) is induced mainly due to air interaction, it remains unaltered with distance (Fig. 6).

The overall distribution of the droplet sizes and the respective velocities is depicted in Fig. 7. The maximum number of droplets is in the size range of 50–150 μm. As the jet penetrates into the crossflow at $\sim 28°$, initially, small-scale waves are formed on the jet surface (wavelength, $\lambda_w \sim 0.28$ mm). The unstable waves shed by forming ligaments (length, $l_{lig} \sim \lambda_w$). These ligaments strip of the surface forming droplets. Therefore, velocity of these droplets at the periphery scales similar to the surface wave transmission rate ($\sim$8 m/s). The droplets in the central region are mainly formed due to column breakup. Therefore, the velocity in the central region (11–14 m/s) is always higher than at the periphery (5–10 m/s), irrespective of the droplet sizes [Fig. 7(a)]. As explained earlier, the number of smaller droplets (25–100 μm) increases as the spray moves further away from the nozzle exit. Accordingly the velocity of these smaller droplets also increases (12–18 m/s) as compared to the near nozzle areas [Fig. 7(b)]. The drift velocity in the crosswise direction (v_x) is very small in any case ($\sim$1–4 m/s) and remains unaltered with distance.

C. Impact of spray on surfaces

As the spray is used to cool the tool (burr), it is also crucial to understand the impact dynamics. The impact of the spray was studied on hard substrates (glass slides) at different locations from the nozzle exit. The slides were washed thoroughly using isopropanol to avoid any contamination and placed at various distances (10–30 mm from o), where the spray structures were already characterized (Sec. II). Initially, the spray impacts the dry surface of the glass slide and gets deposited forming a thin liquid film on the surface [Fig. 8(a)]. The spray is asymmetric at the point of contact. Therefore, the film thickness increases rapidly (at a rate of $\sim$0.3 m/s) due to the continuous deposition of the sprayed droplets. The film grows up to a maximum

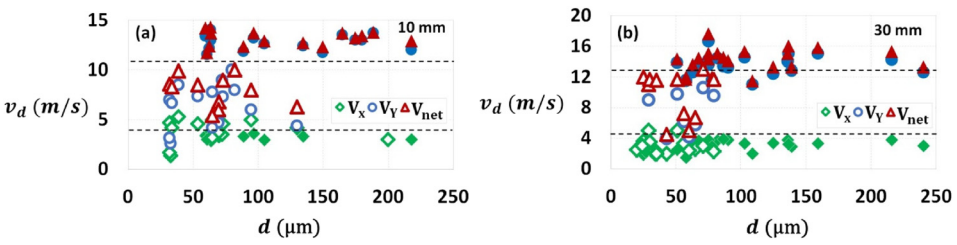

FIG. 7. Variation of velocities of the droplets with droplet sizes (diameter) (unfilled symbols represent droplets in the peripheral region of the spray and filled symbols represent droplets in the central region).

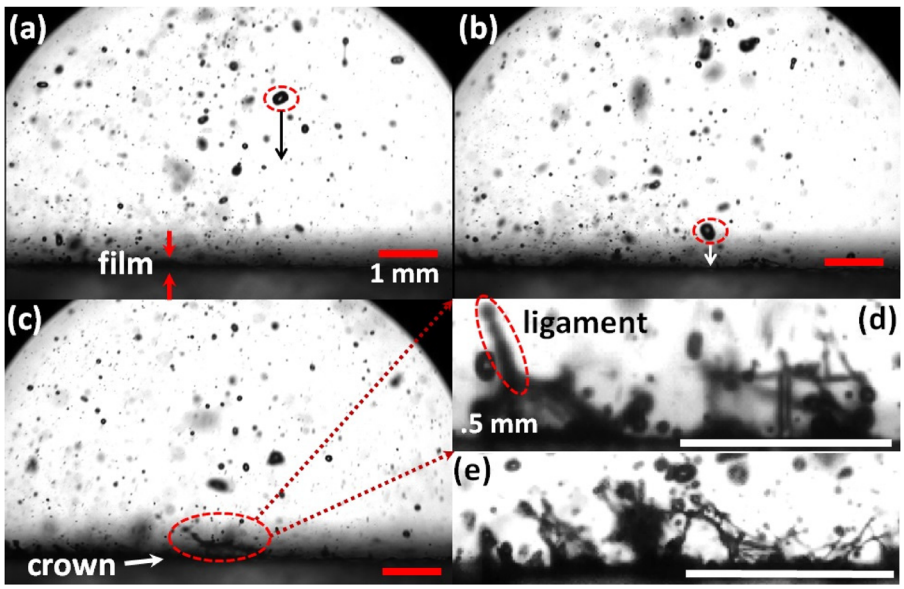

FIG. 8. Impact dynamics of spray on a glass substrate: (a) film formation, (b) droplet impact the film, (c) crown formation, (d) ligament formation, and (e) multiple crown formation.

thickness ($t_{film} \sim 80\,\mu m$). The sprayed droplets then impinge this thin film and form crown-type structures [Fig. 8(c)]. The dynamics of such crown-type structures have been rigorously studied earlier.[23–26] As the droplets impinges on the film due to its inertia, the residual energy subsequent to viscous dissipation leads to the growth of the crown-type structure (Fig. 9). The rate of viscous dissipation ($\mu \frac{d^2v}{dy^2} \sim O(10^4)$ kgm^2/s^2; μ and v are viscosity and velocity of the droplets) in the film is smaller than the inertia ($\rho \frac{dv}{dt}$; ρ is density of the droplet) by an order of magnitude and hence the residual inertia is quite significant to develop the crown in both the radial ($w \sim 150–300\,\mu m$) and axial ($h \sim 50–90\,\mu m$) directions [Fig. 9(d)]. However, the rate of growth is higher radially as compared to the axial growth $\left(\frac{dw}{dt} \sim 3\frac{dh}{dt}\right)$. As the crown expands it is subjected to capillary instabilities which are perceived as waves on the periphery [Fig. 9(e)]. The liquid accumulates at the periphery of the crown and leads to the formation of ligaments [Fig. 9(f)]. These ligaments grow and undergo Rayleigh–Plateau type breakup [$l_{lig}/d_{lig} \sim O(10^2)$] into daughter droplets (diameter, $d_d \sim 10–120\,\mu m$). The daughter droplets then drift away with velocities of $\sim O(10^1)$ m/s (mean velocity ~ 1.9 m/s). Interestingly, the droplets with kinetic energy less than $\sim O(10^{-9})$ J do not undergo splashing phenomena due to insufficient residual energy. These droplets stick to the surface and only increase the thickness of the liquid film. Further impact of sprayed droplets causes multiple collisions and overlapping of multiple crowns [Fig. 8(e)].

The thickness of the deposited liquid film (t_{film}) does not change appreciably as the substrate is moved away from the nozzle exit (10–30 mm). The spray cone expands as it progresses forward and should typically increase the area of impact at different distance away from the nozzle exit. However, the expansion in the spray area is very small due to small length scale of the spray system, and hence, the effect is almost negligible in the current study.

The main concern is to prevent cross-contamination in dentistry. In dental settings, the distance between the patient and the operator is usually very less (<40 cm).[1] The daughter droplets formed after jet breakup are found to be $\sim 35–75\,\mu m$ and these droplets traverse at an average velocity of ~ 1.9 m/s. Therefore, droplets would rise to a

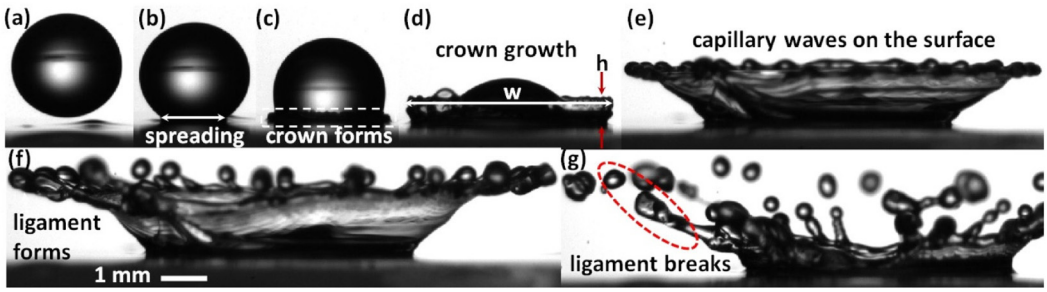

FIG. 9. Dynamics of a droplet impacting a thin film on a glass substrate: (a) impacting droplet, (b) spreading of the droplet, (c) initiation of the crown, (d) radial and axial growth of the crown, (e) capillary instability identifies as waves on the periphery of the crown, (f) ligament formation on the periphery, and (g) breakup of ligaments.

distance of 7–20 cm, which is close proximity to the dentist from the oral cavity of the patient. Moreover, most of the droplets are $<50\ \mu$m, which remains suspended in ambient as aerosols for hours prior to settling to the ground.

As a future scope, several modifications can be made in the nozzle design to reduce the rebounce of droplets after impacting a surface in order to prevent the formation of bio-aerosols in dental environment.

V. CONCLUSIONS

In this work, we have characterized a spray system used for cooling dental airotors. Different types of breakup modes like bag breakup and Rayleigh–Plateau breakup are identified in the process. The spray is more uniform in the peripheral region due to severe shear stripping with an average droplet size of 50 μm and velocity of 8 m/s. Furthermore, the spray is more uniform as it moves away from the nozzle due to better atomization. For the second part, the impact of the spray upon substrates was studied. Most of the droplets sprayed upon a substrate leads to the deposition of a thin film on the surface. Some droplets with higher energy rebounce after the impact and do not contribute to the film formation. The droplets then impact the film and form crown-type structure, which is followed by ligament formation and breakup. The daughter droplets formed of ligaments as well as the rebounding parent droplet drifts away from the surface with velocities of $\sim O(10^1)$ m/s. It can be inferred from the characterized data that chance of transmission of disease is very high in such spray systems used for cooling dental airotors. Therefore, it is highly essential to improvise the design of the spray nozzle minimize the risk of cross-transmission in dental environment. As a future scope, appropriate design modifications will be made in the nozzle and further investigations will be carried out to examine the cooling efficiency of the modified spray using heated substrates. The future aim is to achieve efficient cooling of the tool and reduced rebounce of the daughter droplets.

ACKNOWLEDGMENTS

We thank Science and Engineering Research Board (SERB), India, for funding this project under the Grant No. SRG/2020/000678.

AUTHOR DECLARATIONS

Conflict of Interest

The authors have no conflicts to disclose.

Author Contributions

Binita Pathak: Conceptualization (lead); Data curation (lead); Funding acquisition (lead); Investigation (lead); Project administration (lead); Supervision (lead); Writing – original draft (lead); Writing – review & editing (lead). **Saurabh Yadav:** Data curation (supporting); Visualization (supporting).

DATA AVAILABILITY

The data that support the findings of this study are available from the corresponding author upon reasonable request.

REFERENCES

[1]L. Bourouiba, "Turbulent gas clouds and respiratory pathogen emissions: Potential implications for reducing transmission of COVID-19," JAMA **323**(18), 1837–1838 (2020).
[2]J. M. Weaver, "Confirmed transmission of hepatitis C in an oral surgery office," Anesth. Prog. **61**(3), 93–94 (2014).
[3]K. Ishihama, S. Iida, H. Koizumi, T. Wada, T. Adachi, E. Isomura-Tanaka, T. Yamanishi, A. Enomoto, and M. Kogo, "High incidence of blood exposure due to imperceptible contaminated splatters during oral surgery," J. Oral Maxillofac. Surg. **66**(4), 704–710 (2008).
[4]A. Clark, "Bacterial colonization of dental units and the nasal flora of dental personnel," Proc. R. Soc. Med. **67**, 1269–1270 (1974).
[5]I. Abramovitz, A. Palmon, D. Levy, B. Karabucak, N. Kot-Limon, B. Shay, A. Kolokythas, and G. Almoznino, "Dental care during the coronavirus disease 2019 (COVID-19) outbreak: Operatory considerations and clinical aspects," Quintessence Int. **51**(5), 418–429 (2020).
[6]J. R. Allison, D. C. Edwards, C. Bowes, K. Pickering, C. Dowson, S. J. Stone, J. Lumb, J. Durham, N. Jakubovics, and R. Holliday, "The effect of high-speed dental handpiece coolant delivery and design on aerosol and droplet production," J. Dent. **112**, 103746 (2021).
[7]A. Adhikari, S. Kurella, P. Banerjee, and A. Mitra, "Aerosolized bacteria and microbial activity in dental clinics during cleaning procedures," J. Aerosol Sci. **114**, 209–218 (2017).
[8]R. E. Micik, R. L. Miller, M. A. Mazzarella, and G. Ryge, "Studies on dental aerobiology: I. Bacterial aerosols generated during dental procedures," J. Dent. Res. **48**(1), 49–56 (1969).
[9]S. Dutil, A. Mériaux, M. C. de Latrémoille, L. Lazure, J. Barbeau, and C. Duchaine, "Measurement of airborne bacteria and endotoxin generated during dental cleaning," J. Occup. Environ. Hyg. **6**(2), 121–130 (2008).
[10]A. Sergis, W. G. Wade, J. E. Gallagher, A. P. Morrell, S. Patel, C. M. Dickinson, N. Nizarali, E. Whaites, J. Johnson, O. Addison, and Y. Hardalupas, "Mechanisms of atomization from rotary dental instruments and its mitigation," J. Dent. Res. **100**(3), 261–267 (2021).
[11]N. Innes, I. G. Johnson, W. Al-Yaseen, R. Harris, R. Jones, S. Kc, S. McGregor, M. Robertson, W. G. Wade, and J. E. Gallagher, "A systematic review of droplet and aerosol generation in dentistry," J. Dent. **105**, 103556 (2021).
[12]K. S. Siddharth, M. V. Panchagnula, and T. J. Tharakan, "Effect of gas swirl on the performance of a gas-centered swirl co-axial injector," Atomization Sprays **27**(8), 741 (2017).
[13]*Handbook of Atomization and Sprays: Theory and Applications*, edited by N. Ashgriz (Springer Science & Business Media, 2011).
[14]A. Davanlou, J. D. Lee, S. Basu, and R. Kumar, "Effect of viscosity and surface tension on breakup and coalescence of bicomponent sprays," Chem. Eng. Sci. **131**, 243–255 (2015).
[15]R. A. Dafsari, H. J. Lee, J. Han, D.-C. Park, and J. Lee, "Viscosity effect on the pressure swirl atomization of an alternative aviation fuel," Fuel **240**, 179–191 (2019).
[16]A. P. Kulkarni, T. Megaritis, and L. C. Ganippa, "Insights on the morphology of air-assisted breakup of urea-water-solution sprays for varying surface tension," Int. J. Multiphase Flow **133**, 103448 (2020).
[17]J. Mallory and P. E. Sojka, "On the primary atomization of non-Newtonian impinging jets: Volume I experimental investigation," Atomization Sprays **24**(5), 431 (2014).
[18]G. M. Faeth, L. P. Hsiang, and P. K. Wu, "Structure and breakup properties of sprays," Int. J. Multiphase Flow **21**, 99–127 (1995).
[19]A. H. Lefebvre and V. G. McDonell, *Atomization and Sprays* (CRC Press, 2017).
[20]J. C. Beale and R. D. Reitz, "Modeling spray atomization with the Kelvin-Helmholtz/Rayleigh-Taylor hybrid model," Atomization Sprays **9**(6), 623 (1999).
[21]S. K. Vankeswaram and S. Deivandren, "Size and velocity characteristics of spray droplets in near-region of liquid film breakup in a swirl atomizer," Exp. Therm. Fluid Sci. **130**, 110505 (2022).

[22]I. K. Zwertvaegher, M. Verhaeghe, E. Brusselman, P. Verboven, F. Lebeau, M. Massinon, B. M. Nicolaï, and D. Nuyttens, "The impact and retention of spray droplets on a horizontal hydrophobic surface," Biosyst. Eng. **126**, 82–91 (2014).
[23]I. V. Roisman, R. Rioboo, and C. Tropea, "Normal impact of a liquid drop on a dry surface: Model for spreading and receding," Proc. R. Soc. London, Ser. A **458**(2022), 1411–1430 (2002).
[24]F. Yeganehdoust, R. Attarzadeh, I. Karimfazli, and A. Dolatabadi, "A numerical analysis of air entrapment during droplet impact on an immiscible liquid film," Int. J. Multiphase Flow **124**, 103175 (2020).
[25]C. Josserand, P. Ray, and S. Zaleski, "Droplet impact on a thin liquid film: Anatomy of the splash," J. Fluid Mech. **802**, 775–805 (2016).
[26]Z. Che and O. K. Matar, "Impact of droplets on immiscible liquid films," Soft Matter **14**(9), 1540–1551 (2018).